Green Chemistry

PAPER

View Article Online
View Journal | View Issue

Cite this: *Green Chem.*, 2025, **27**, 650

Interactions, properties and lipid digestibility of attractive Pickering emulgels formed by sequential addition of oppositely charged nanopolysaccharides†

Shasha Guo,[a,b,c] Jun Li,[b] Xingxiang Ji,[a] Wenjuan Jiao,[d] Zhangmin Wan,[c] Luyao Huang,[b] Xun Niu,[c] Junhua Xu,[c] Ying Liu,[c] Jianan Zheng,[d] Bin Li,[e] Long Bai,[c,f] Yi Lu *[c,g] and Orlando J. Rojas *[c,h,i]

Emulsion gels (emulgels) have emerged as cost-effective and versatile platforms in formulation engineering. In this study, we introduce Attractive Pickering Emulgels (APEGs), stabilized by the synergistic action of two oppositely charged green nanoparticles, *e.g.*, chitin nanofibers (ChNF) and cellulose nanocrystals (CNC). The CNC, featuring anionic sulfate half-ester groups, and the cationic ChNF, possessing amine groups, form adhesive bridging networks within the continuous aqueous phase, effectively inhibiting oil droplet coalescence. This network supports micro-clustering, significantly increasing the effective droplet volume fraction by entrapping substantial amounts of the continuous phase. Consequently, the emulgels demonstrate a robust viscoelastic response and effectively modulate lipid digestibility, as evidenced by a 30% reduction in free fatty acid (FFA) release at high oil fractions (70 wt%) during *in vitro* digestion. The stabilization mechanism relies on noncovalent interactions and nanoparticle coassembly, validated through quartz crystal microgravimetry and molecular dynamics simulations. APEGs present significant potential for advancing sustainable nanotechnologies in pharmaceutical, food, and health formulations.

Received 8th November 2024,
Accepted 6th December 2024

DOI: 10.1039/d4gc05700g

rsc.li/greenchem

Green foundation

1. This work reports the first all nanopolysaccharide-based Attractive Pickering Emulsion Gel (APEG) developed using a two-step sequential addition method. The inherently green nature of polysaccharide nanoparticles highlights their potential applications in pharmaceutical, food, and health formulations.
2. A simple strategy involving sequential addition of nanochitin and nanocellulose can initiate interdroplet interactions through an electrostatic attraction-induced bridging effect. This approach enhances the emulgel rheological properties of the emulgel by over 10 times, opens the way to 3D printed structures with minimum particle dosage, and reduces free fatty acid (FFA) release during *in vitro* digestion.
3. In future work, the APEG system can be expanded to a broader range of natural polymers and nanoparticles, such as proteins, alginates, DNA. These materials are particularly promising for applications in 3D-printed healthy foods.

[a]*State Key Laboratory of Biobased Material and Green Papermaking, Qilu University of Technology, Shandong Academy of Sciences, Jinan, 250353, China*
[b]*State Key Laboratory of Pulp and Paper Engineering, South China University of Technology, Guangzhou 510640, China*
[c]*Bioproducts Institute, Department of Chemical & Biological Engineering, The University of British Columbia, 2360 East Mall, Vancouver, BC, Canada V6T 1Z3. E-mail: orlando.rojas@ubc.ca, luyi@ipe.ac.cn*
[d]*Sericulture & Agri-food Research Institute Guangdong Academy of Agricultural Sciences, Key Laboratory of Functional Foods, Ministry of Agriculture and Rural Affairs, Guangdong Key Laboratory of Agricultural Products Processing, Guangzhou, 510610, China*
[e]*CAS Key Laboratory of Biofuels, Qingdao Institute of Bioenergy and Bioprocess Technology, Chinese Academy of Sciences, Qingdao 266101, China*
[f]*Key Laboratory of Bio-based Material Science & Technology (Ministry of Education), Northeast Forestry University, Harbin 150040, P.R. China*
[g]*CAS Key Laboratory of Green Process and Engineering, Institute of Process Engineering, Chinese Academy of Sciences, Beijing 100190, PR China*
[h]*Department of Chemistry, The University of British Columbia, 2036 Main Mall, Vancouver, BC, Canada V6T 1Z1*
[i]*Department of Wood Science, The University of British Columbia, 2900-2424 Main Mall Vancouver, BC, Canada V6T 1Z4*

† Electronic supplementary information (ESI) available. See DOI: https://doi.org/10.1039/d4gc05700g

Introduction

Pickering emulsion gels (emulgels) integrate the structural benefits of both emulsions and gels, forming stable multiphase systems through the irreversible interfacial packing of colloidal particles.[1] This Pickering stabilization imparts resistance to coalescence, Ostwald ripening, and phase separation, resulting in ultra-stable systems with promising mechanical properties and complex hierarchical structures.[2] These features make Pickering emulgels highly relevant across complex fluids, materials science, pharmaceuticals, and food technology.[3–5]

Engineering interdroplet interactions in Pickering emulgels is crucial for enhancing their viscoelastic properties, which is essential for applications like 3D printing and cell culturing. These interactions can be either repulsive or attractive. Repulsive emulgels typically involve single-type Pickering stabilizers, where electrostatic repulsion between charged stabilizing particles dictates the rheological behavior. This behavior is influenced by the type of stabilizer used and the volume fraction of the dispersed phase. For instance, high internal phase emulsions (with internal phase fractions greater than 74%) exhibit significantly higher viscosity compared to regular emulsions due to the densely packed droplets, which kinetically trap the multiphase system and limit droplet diffusion, resulting in predominantly elastic behavior.[6]

Conversely, attractive Pickering emulgels (APEGs) form through the aggregation of oil droplets into fractal clusters due to attractive interactions, resulting in the creation of physically cross-linked networks.[7] The clustering of oil droplets in APEGs significantly enhances their rheological properties. Unlike repulsive emulgels, where the effective oil volume fraction is dictated by particle repulsion, APEGs exhibit increased effective oil volume fractions as droplet clustering occurs. This clustering enables the development of elastic properties at much lower oil fractions, even below the threshold of random close packing.[8]

APEGs, often involving chemical modification of stabilizing particles, are underexplored in current literature. Zein nanoparticles have been demonstrated to alter the interfacial properties of anionic emulsifiers in oil-in-water emulsions, promoting the formation of droplet-bridging networks.[9] APEGs can also be formed in water-in-oil emulsions using α,ω-diamino functionalized polymers that interact with carboxyl-functionalized nanoparticle-stabilized droplets.[10,11] In these systems, controlling the salt concentration and pH allows fine-tuning of the electrostatic attractions that govern emulsion stability.[12–15] To the best of our knowledge, no efforts have been undertaken to develop all green nanoparticle-based APEG systems. Nevertheless, in the past decade, the utilization and valorization of green nanoparticles in emulsion formulation have become a primary driving force for advancing green chemistry pertaining to human well-being, including food, pharmaceutical, and biomedical applications.[5,16–19]

In this work, we present a Pickering emulgel utilizing fully biobased components. Chitin nanofibers (ChNF) are employed as the primary stabilizer of the initial Pickering emulsion. Subsequent addition of cellulose nanocrystals (CNC) to the aqueous phase creates a secondary emulsion gel, where droplets are interconnected by polysaccharide "bridging" networks. Both ChNF and CNC, as renewable nanomaterials, have garnered significant interest in the formulation of Pickering emulsions,[20,21] aligning with ever-increasing demands in green chemistry and sustainability.[22] These nanomaterials strongly adsorb at the water–oil interface, effectively preventing droplet coalescence.[23,24] Additionally, chitin and cellulose nanoparticles are cost-effective[25,26] and non-digestible, making them suitable sources of dietary fibers.[27]

Compared to traditional methods aimed at enhancing phase dispersion and inducing gelation in emulsions, structuring networks through electrostatic interactions is simpler and more effective. In this context, negatively charged CNCs are promising candidates to interact with positively charged ChNFs.[28,29] However, the single-step mixing of ChNF and CNC results in instantaneous particle aggregation, where larger particulate complexes are less efficient for emulsion stabilization.[30] To date, creating dietary fiber-based Pickering emulsions with minimal nanoparticle content while achieving superior rheological properties remains a significant challenge.

To achieve bridging flocculation of droplets without particle aggregation, we adopt a sequential preparation strategy for robust APEGs. Initially, positively charged ChNF is selected as the Pickering stabilizer for oil droplets. Subsequently, CNC nanoparticles are added in a secondary step to electrostatically couple with the ChNF-stabilized droplets. This sequential addition aims to ensure that negatively charged CNCs bind selectively to neighboring oil droplets, facilitating the formation of APEGs. Our strategy demonstrated a facile yet efficient protocol for adjusting the rheological properties of all nanopolysaccharide-based systems at low particle dosages, which is essential for developing customer product formulations from green and sustainable chemicals. In this work, we showcase that such controlled droplet clustering can regulate lipid digestibility in the gastrointestinal tract, offering significant implications for controlled and targeted release applications.

Results and discussion

Attractive Pickering emulgels (APEGs)

APEGs were prepared using a sequential protocol that included (Fig. 1a) (i) emulsification of oil droplets in the continuous aqueous phase using ChNF as the stabilizer, followed by (ii) bridging of oil droplets by adding oppositely charged CNC. While commercial sunflower oil contains some biosurfactants, these do not exhibit sufficient interfacial activity to stabilize the emulsions. ChNF was chosen as a Pickering stabilizer due to its effective adsorption and self-assembly at interfaces. Recent studies have demonstrated that ChNF-stabilized Pickering emulsions can accommodate high internal (oil) phase content, attributed to significant hydrophobicity from

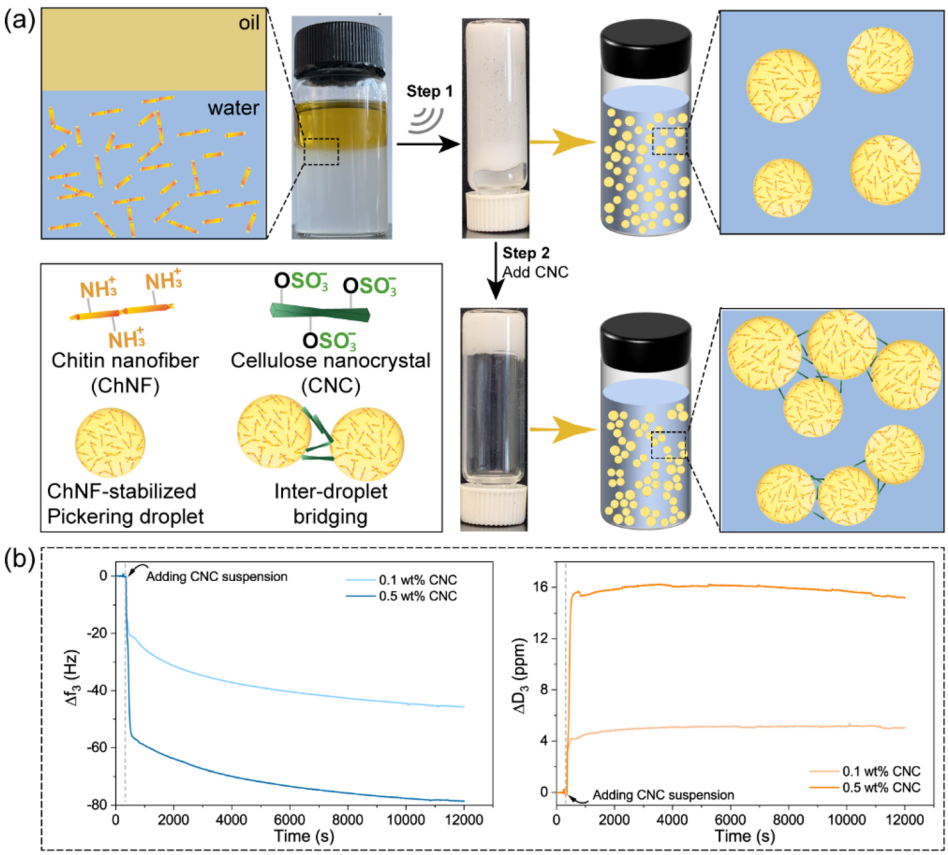

Fig. 1 Principles of attractive Pickering emulsion gels (APEG). (a) Attractive Pickering emulsion gels (APEG) are formed through ChNF-CNC interfacial complexation through a sequential addition approach. Initially, ChNF-stabilized Pickering emulsions are generated by vigorous mixing (step 1). Subsequently, oppositely charged CNC is added, facilitating interfacial electrostatic complexation and inter-droplet bridging (step 2). APEG exhibits significantly enhanced viscoelasticity, as demonstrated in the inverted vial test. (b) ChNF–CNC attractive interactions measured by Quartz-Crystal Microgravimetry with Dissipation (QCM-D): The attractive interactions between ChNF and CNC are quantified using QCM-D. The shift in frequency (left) and dissipation (right) over time illustrates the electrostatic complexation dynamics when CNC dispersed in water is added to ChNF films.

acetylamine groups.[24] In this work, CNC loading is demonstrated to result in a highly viscous APEG. CNC effectively bridges oil droplets into an interconnected network without displacing or disrupting the interfacially adsorbed nanochitin. Low-energy agitation leads to the formation of a droplet network (Fig. S1 and S2†).[31] The properties of Pickering emulsions differ significantly when prepared using a single-batch addition, which does not enhance the droplet volume fraction.[30]

Interparticle and interdroplet attraction

Quartz-crystal microgravimetry. The attraction between oppositely charged CNC and ChNF originates from electrostatic forces. Quartz-crystal microbalance with dissipation (QCM-D) was employed to monitor real-time interactions between these two polysaccharide nanoparticles. Typically, an increase in QCM frequency shift (Δf) indicates mass release from the interface, while changes in dissipation (ΔD) reflect the softness of the adsorbed layer.

Upon adding an aqueous CNC suspension to a ChNF-coated sensor, both frequency and dissipation exhibited immediate and significant shifts, illustrating instantaneous interparticle attraction (Fig. 1b). Higher CNC concentrations resulted in more pronounced changes in both frequency and dissipation. Initially (Δf at t ~0 s), significant CNC adsorption was observed, followed by a second regime of steady nanoparticle adsorption until reaching equilibrium (t ~12 000 s). Changes in dissipation and mass were notably significant only during the initial adsorption stage (Fig. 1b and S3†). These observations indicate strong CNC-ChNF interactions during the initial stage, with subsequent adsorption likely driven by physical stacking and particle reorganization.[32]

The interactions between CNC and ChNF directly influenced changes in particle charge density. Balancing the charge density of CNC and ChNF nanoparticles was crucial for achieving effective interdroplet attraction. In this study, the ζ-potential of pristine CNC and ChNF nanoparticles was −(53 ± 2.8) and +(97 ± 3.9) mV, respectively. The charge neutralization point was determined at a CNC-to-ChNF ratio of 5 : 1 (w/w), corresponding to 0.5 wt% CNC and 0.1 wt% ChNF (Fig. 2a).

The interparticle attraction was translated into interdroplet interactions within Pickering emulsion systems through a

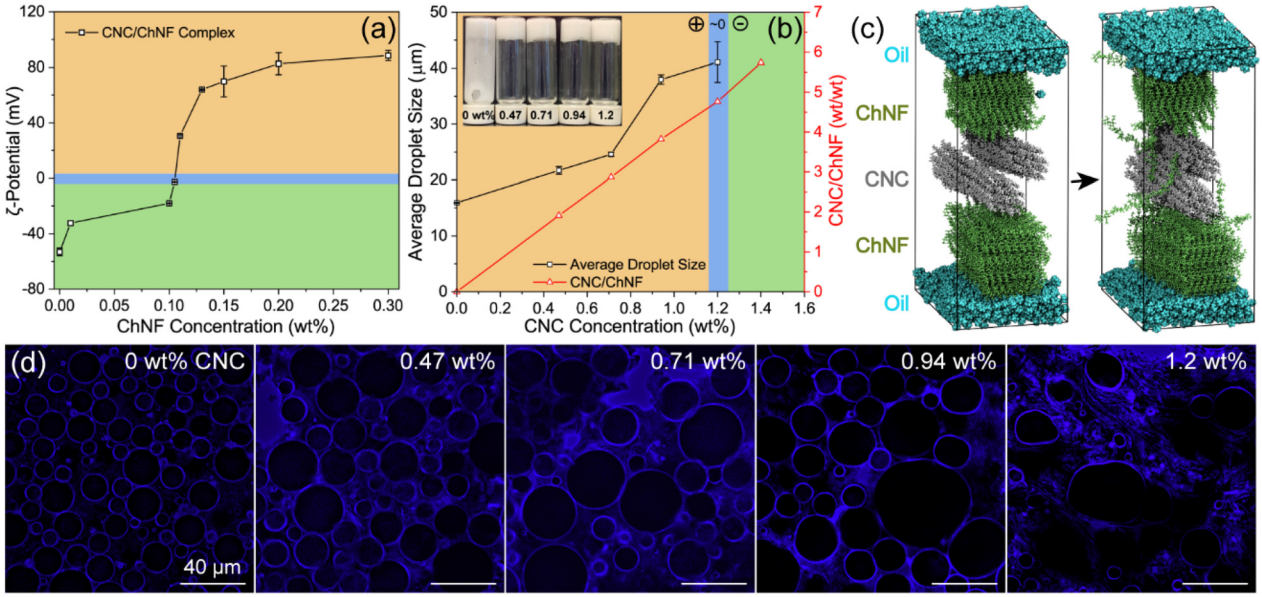

Fig. 2 (a) Changes in ζ-potential of an aqueous CNC (0.5 wt%) suspension were observed upon incremental addition of ChNF. (b) The mean droplet diameter (D_{32}) and visual appearance of Pickering emulsions were evaluated across a range of CNC loadings, from 0 to 1.4 wt%. The red line denotes the specified CNC/ChNF ratio in the emulsions. (c) Molecular dynamic simulations were employed to investigate the interactions between CNC and ChNF at the oil–water interface. (d) Fluorescence microscopy images depict ChNF-stabilized oil-in-water Pickering emulsions with varying CNC loadings (0, 0.47, 0.71, 0.94, and 1.2 wt%). The aqueous phase is visualized with Calcofluor white dye.

sequential addition approach, resulting in APEG formation. Initially, a conventional Pickering emulsion system was achieved by vigorously mixing the ChNF suspension with the oil phase (Fig. 1a, step 1), where the oil–water interfaces were occupied by positively charged ChNF.

In the subsequent step (CNC loading, Fig. 1a, step 2), the negatively charged sulfate half-ester groups on CNC electrostatically bound to the amine groups of ChNF. Ideally, each CNC particle should be capable of simultaneously binding to two neighboring droplets, thereby acting as a bridging agent, as depicted in step 2.

To confirm the role of CNC in bridging, a series of experiments were conducted where ChNF-stabilized emulsions remained liquid-like in the absence of CNC (inset image: 0 wt% CNC, Fig. 2b). Excessive CNC led to charge reversal and phase separation (1.4 wt% CNC, Fig. S4a†). Highly viscous APEGs were successfully formed only with intermediate CNC additions following the sequential addition approach.

The electrostatic complexation between ChNF and CNC at the oil–water interface was validated by monitoring changes in droplet size. With increasing CNC loading, oil droplets progressively enlarged and clustered (interdroplet bridging, Fig. 2b and Fig. S4b†), eventually resulting in severe droplet coalescence at excessive CNC concentrations.[33] The apparent oil droplet size increased from 16 to 41 μm when the CNC concentration reached 1.2 wt%.

The micromorphology of APEGs was further examined using fluorescence microscopy (Fig. 2d and Fig. S5, S6†), where polysaccharide nanoparticles and the oil phase were stained in blue (Calcofluor White) and red (Nile red), respectively. In the absence of CNC (0 wt% CNC), ChNFs were firmly adsorbed at the oil–water interface, with minimal fluorescence observed in the bulk dispersion due to strong Pickering stabilization.

At intermediate CNC concentrations, electrostatic complexation had minimal impact on droplet morphology but induced a viscosifying effect through bridging (Fig. 2d). Fluorescence images revealed CNCs adsorbed as bridging agents with an uneven spatial distribution around the oil droplets. Irreversible interactions between CNC and interfacially-adsorbed ChNFs promoted network formation among droplet clusters (Fig. 2d for 0.47, 0.71, and 0.94 wt% CNC), maintaining spherical droplet shapes. Upon reaching charge neutrality (1.2 wt% CNC), droplets began to deform (Fig. 2d, blue area in Fig. 2a and b), but no phase separation was observed.

Molecular dynamic (MD) simulation. Molecular dynamics (MD) simulations were employed to investigate interdroplet electrostatic complexation (Fig. 2c). Incremental addition of CNC facilitated bridging between ChNF-stabilized droplets without inducing interfacial destabilization (*i.e.*, ChNF desorption). Specifically, ChNF remained firmly adsorbed at the oil–water interface, influencing droplet size. Simulation results were consistent with experimental observations, demonstrating that emulsified oil droplets formed an interconnected network due to attractive forces between neighboring droplets.

However, excessive CNC addition (1.4 wt%) to ChNF-stabilized emulsions resulted in phase separation due to droplet coalescence (Fig. S4a†). A visible layer of oil is separated from the emulsion. The concentration of CNC corresponded to the negatively charged state of the suspension (green area in

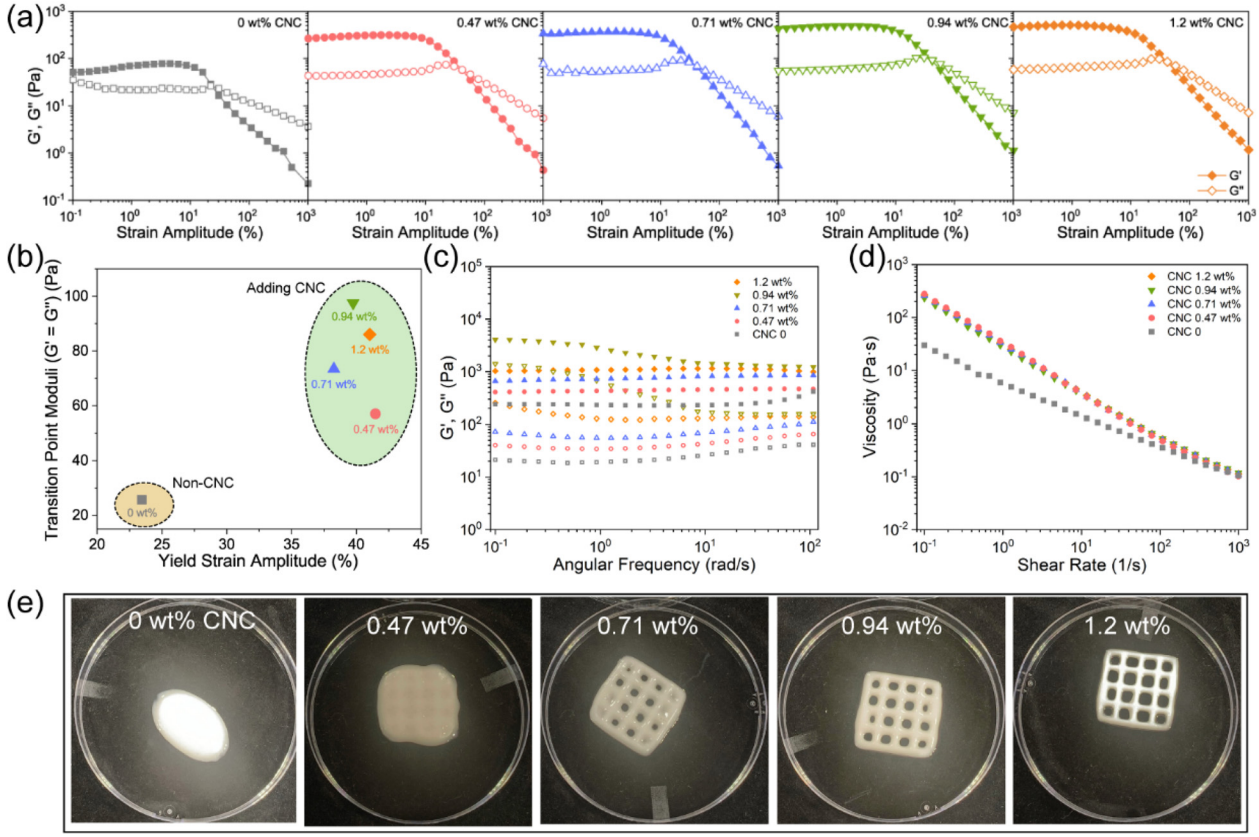

Fig. 3 (a) Strain amplitude sweep, (b) transition strain amplitude, (c) frequency sweep, and (d) steady-state flow curves of emulsions prepared with different CNC concentrations (0, 0.47, 0.71, 0.94, and 1.2 wt%). G' and G'' represent the elastic (storage) and viscous (loss) moduli, respectively. (e) 3D-printed structure obtained from the respective emulsions.

Fig. 2a). This finding suggests that the CNC/ChNF ratio at charge neutralization represents the upper limit for successful APEG formulation.

Viscoelastic properties of APEGs

The addition of CNC for interdroplet bridging and complexation significantly enhanced the viscoelastic properties of the emulsion, as demonstrated by oscillatory and rotational shear tests (Fig. 3a). The critical strain amplitude, characterized by the maximum range of the linear viscoelastic region (LVR), showed notable improvements. Pickering emulsions stabilized solely with ChNF exhibited a critical strain amplitude of 12%. With incremental CNC loading, these values decreased gradually to 2%, indicating enhanced stability.

All tested emulsions displayed suitable viscoelastic behavior within the LVR ($G' > G''$). Even at low levels of CNC addition, there was a significant enhancement in the storage modulus (Fig. S7†). Higher G' values indicated a stronger network structure, directly attributed to the reinforcement of droplet networking by CNC.[34]

All emulsions displayed nonlinear strain-thinning as they transitioned from the linear viscoelastic region (LVR) to the nonlinear viscoelastic region. As observed in previous comprehensive studies,[35] the samples exhibited a typical weak strain overshoot behavior of type III, characterized by an increase in the loss modulus (G'') while the storage modulus (G') remains relatively stable. This overshoot in the loss modulus likely stems from the emulsions' complex structure resisting deformation up to a certain strain threshold.

Beyond this critical strain, the complex structure was disrupted, indicated by the point where G' equals G'' ($G' = G''$), marking the yield point. This critical transition reflects the point where the emulsion's structure could no longer withstand further deformation under external strain.[36] As depicted in Fig. 3b, the moduli and strain amplitudes at the transition point were higher in CNC-added emulsions compared to those without CNC (notably, the 0.94 wt% CNC emulsion exhibited the highest modulus). Eventually, the network structure broke down, transitioning into a state where the fluid began to flow ($G' < G''$). This breakdown highlights the robust internal structure of the droplet network, particularly evident in the 0.94 wt% CNC emulsion, which showed the highest modulus at the yield point.

Frequency sweep tests were conducted at a strain amplitude of 0.5%, within the linear viscoelastic region (LVR). The results clearly indicated that the storage modulus (G') was consistently higher than the loss modulus (G'') across all frequencies for the five emulsions tested (Fig. 3c). Notably, the emulsion con-

taining 0.94 wt% CNC exhibited enhanced stability, characterized by a higher G' value at lower frequencies. This improved elasticity can be attributed to effective droplet bridging and increased droplet-droplet friction facilitated by the CNC at this concentration.[37] Furthermore, the addition of CNC led to increased elastic behavior and higher apparent viscosity (Fig. 3d), primarily due to the transformation of spherical droplets into non-spherical clusters. Non-spherical objects tend to have larger hydrodynamic diameters and occupy greater volumes compared to their spherical counterparts.[38]

The excellent performance and unique viscoelastic properties of APEG systems are anticipated to facilitate straightforward processing and the tailored design of functional materials, such as through 3D printing, as illustrated in Fig. 3e. During shearing, all emulsions were extruded continuously with a viscous modulus (G'') exceeding the elastic modulus (G'), without any clogging issues. Post-extrusion, emulsions containing >0.71 wt% CNC regained their viscoelasticity and maintained their printed 3D structures. CNC's role in bridging the droplet network underscores these emulsions' suitability for 3D printing, offering a versatile platform for creating customized foodstuffs.

Emulgels with varying oil fractions

The method used to prepare the APEGs is generally applicable to a wide range of oil fractions. This concept is of particular interest to functional food, since both nanochitin and nanocellulose are natural polysaccharides. Thus, the as-prepared APEGs can serve as dietary fiber ingredients in foodstuff.

CNC/ChNF-based APEGs were successfully created with oil fractions ranging from 40% to 70%, stabilized initially by 0.25 wt% ChNF in the emulsion (step 1). All emulsions exhibited high viscoelasticity (as demonstrated by inverted vial tests) and stability (no phase separation) (Fig. 4a). As the oil fraction increased, the size of oil droplets also increased gradually (Fig. 4d). At a constant concentration of ChNF, higher oil fractions approached the surface coverage limit of ChNF, potentially causing more frequent droplet collisions during ultrasonication and, consequently, leading to coalescence.

Across all oil ratios, the emulsions exhibited gel-like behavior ($G' > G''$) under small oscillatory shear amplitudes, transitioning to a liquid-like state at the transition point (Fig. S8a†). Emulsions with 40 wt% oil had the highest amplitudes at this transition, while those with 70 wt% oil showed the highest modulus (Fig. 4b). The loss factor ($\tan \delta = G''/G'$) peaked at a 70 wt% oil fraction (Fig. 4c). Detailed strain sweeps and viscosity data are provided in Fig. S8.† Generally, APEGs with a high internal phase volume (70 wt%) displayed dense droplet packing and high shear resistance, advantageous for extrusion in 3D printing. Notably, viscosities in emulsions with 40%, 50%, and 60% oil fractions were approximately one order of magnitude higher than those before CNC addition (Fig. 4 and Fig. S9†), indicating significant droplet clustering. This clustering entrapped the continuous aqueous phase within the oil droplets, resulting in a steep viscosity increase due to the

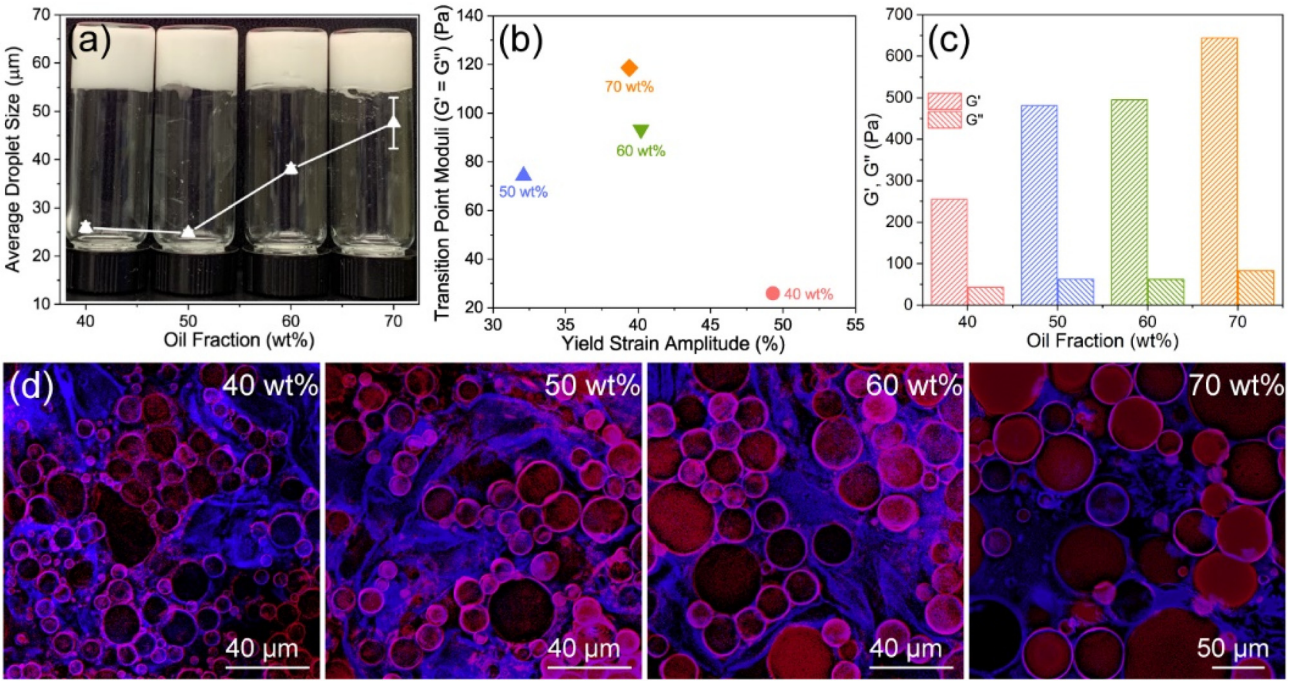

Fig. 4 (a) Visual appearance, average droplet size, and (b) yield strain amplitude of Pickering emulsions prepared with different fractions of oil. (c) Comparison of elastic (G') and viscous (G'') moduli at strain amplitude = 1.28%. (d) Fluorescence microscopy images of ChNF-stabilized oil-in-water Pickering emulsions at different oil fractions (40, 50, 60, and 70 wt%). The oil phase and the ChNF/CNC complexes were stained following the standard procedure using Nile red and Calcofluor white, respectively.

higher effective volume fraction of the oil phase.[7] Therefore, controlling oil droplet clustering through interdroplet interactions is a strategy to achieve gels with specific rheological properties.

Free fatty acid (FFA) release

To evaluate the impact of oil droplet clustering on FFA release, APEGs with varying oil fractions were subjected to a 3-phase digestion process mimicking conditions in the mouth, stomach, and small intestine. During pancreatic lipase hydrolysis of triglycerides, FFAs are produced along with monoacylglycerols and hydrogen ions. The amount of NaOH required to maintain pH 7.0 in the small intestine phase, determined through titration, can quantify triglyceride hydrolysis and FFA release.

FFA release during small intestinal digestion was rapid within the initial 20 minutes for all analyzed APEGs (Fig. 5a). After 120 min of digestion, the emulsion containing 70 wt% oil showed only 30% hydrolysis of FFAs. Conversely, emulsions with 40 wt% oil exhibited a slight increase in FFA hydrolysis, reaching 38%. The size of droplets significantly influenced triglyceride digestion in these emulsions, impacting the surface area available for lipase action.[39] As a result, the digestibility of TAG in the 40 wt% oil Pickering emulsion increased with smaller droplet diameters, which provided a larger total surface area. Moreover, the interconnected network structure within the emulsion could lead to the accumulation of lipid hydrolysis products at the droplet interface, thereby reducing the available surface area for enzymatic hydrolysis by pancreatic lipase and affecting TAG hydrolysis.[27] Interestingly, the ChNF-stabilized Pickering emulsion without CNC exhibited only 22% hydrolysis of free fatty acids (FFAs) (Fig. S10†), which is lower than that observed in APEGs with 70 wt% oil. We propose that the electrostatic attraction in APEGs may render the droplet barrier more susceptible to hydrolysis (Fig. S1 and S2†). The literature indicates variations in FFAs based on the type and concentration of stabilizer used (Fig. S11†). Overall, APEGs demonstrate lower levels of FFAs and accommodate a broader range of oil concentration compared to other emulsified products.

A linear relationship between FFA release and time was observed (Fig. 5b), indicating that FFA release followed first-order kinetic curves with strong linear correlations (coefficients >0.9). Variations were noted in the apparent rate constants across different oil fractions, represented by the absolute slopes of the FFA release kinetics curves. Specifically, emulsions with lower oil fractions underwent FFA digestion more extensively and faster compared to those with higher oil fractions (emulsion with oil fractions of 40%, 50%, 60%, and 70% exhibited apparent rate constants of 0.0305, 0.0297, 0.0289, and 0.0247 s^{-1}, respectively).

Experimental

Materials

Cellulose nanocrystals were purchased from CelluForce (the University of Maine) with dimensions of approximately 6 nm in width and 150–200 nm in length (Fig. S12a†). Fresh crabs (Dungeness) were purchased from a local market in Vancouver, Canada. The chitin nanofibrils were isolated from raw crab shells using a purification protocol based on a pre-

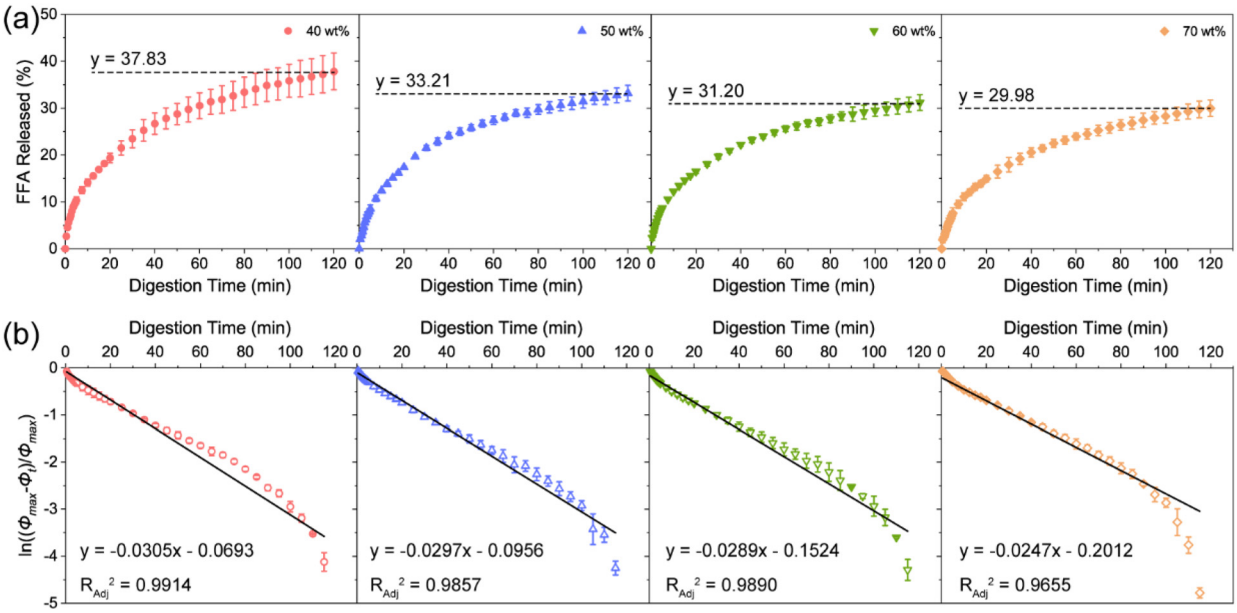

Fig. 5 (a) Levels of total FFAs released from emulsions of different oil fraction (40, 50, 60, and 70 wt%, as noted) after a 120 min digestion in the small digestion phase. (b) Corresponding FFA release data plotted as a first-order kinetics reaction as a function of lipolysis time.

vious study.[30] The obtained ChNFs were about 6 nm in width and 170 nm in length (Fig. S12b†).

Sunflower oil was purchased from a local supermarket and used without further purification. Calcofluor white stain, Nile red, hydrochloric acid, sodium hydroxide, and sodium chlorite were purchased from Sigma-Aldrich (Canada). Analytical-grade chemicals were used in this case.

ChNF/CNC complexes

The ChNF/CNC complexes were prepared by mixing 0.5 wt% CNC suspension with ChNF at varying concentrations, from 0 to 0.3 wt% at a mass ratio of 1 : 1. Vortexing was used to ensure full mixing.

The zeta-potential (ζ-potential) of neat ChNF and CNC, as well as ChNF/CNC complexes, were accessed by electrophoretic light scattering (ZS-90, Malvern Instruments, UK). Freshly prepared samples were used for ζ-potential tests at 25 °C in triplicate. CNC adsorption on ChNF thin films was monitored by a quartz crystal microbalance with dissipation (QCM-D, Q-sense, Biolin Scientific). Details are provided in the ESI.†

Preparation of attractive Pickering emulgels

ChNF-stabilized Pickering emulsions were initially prepared according to our previous work.[31] In a typical Pickering emulsion system, the concentration of ChNF was 0.25 wt%, with an oil-to-water ratio of 4 : 6 (w/w). The mixtures ultrasonicated for 90 s (Sonifier SFX550, Branson Ultrasonics Co., U.S.A.) using a titanium microtip at a power level of 40% of the maximum strength and following alternating on–off cycles (3 s and 2 s, respectively). Additional experiments used emulsions prepared *via* sequential CNC addition by using glass rod stirring. In these experiments, 5.88 wt% CNC gel of a given mass was incorporated in the already prepared ChNF-stabilized Pickering emulsions. The weight ratio of dried CNC and emulsion were 0, 0.47, 0.71, 0.94, 1.2, and 1.4 wt%. It should be noted that additional methods involving stirring and sonication with CNC were compared and presented in the ESI (part 1.3 and Fig. S1†).

Characterization of Pickering emulsions

Droplet size. Emulsion droplet diameter and corresponding size distribution were determined by laser diffraction (MasterSizer 3000, Malvern Instruments, UK). The refractive indices of water and sunflower oil used were assumed to be 1.33 and 1.47, respectively. During the measurement, the emulsion was diluted with Milli-Q water, which effectively diminished the effects of particle and viscosity. This dilution is standard in Dynamic Light Scattering (DLS) analysis to adjust the number concentration of scatters and avoid multiple scattering. The preferred dispersant for emulsion sample preparation should include the stabilizer present in the continuous phase. The mean droplet size was calculated as the volume mean diameter ($D_{32} = \sum n_i d_i^3 / \sum n_i d_i^2$) using the full-size distribution range. The measurements were conducted in quintuplicate using freshly prepared samples.

Emulgel microstructure. A fluorescence microscope (Olympus BX53 with 20× and 60× objective lens) was used to simultaneously identify the ChNF and CNC as well as the sunflower oil. Prior to observation, sunflower oil was dyed with Nile red, and the fibrils were stained with Calcofluor white. The excitation/emission spectrum of Nile Red was 488/539 nm, respectively, while the Calcofluor White stain was 365/435 nm, respectively. The fluorescence signals (red and blue) were processed using the CellSens Dimension software to generate multiple droplets images.

Rheological behavior. Rheological properties of the emulsions were characterized with a rheometer (MCR 302, Anton Paar, Germany) using the parallel plate geometry (PP25) with a gap distance of 0.5 mm. The sample remained at rest for at least 1 min before carrying out the test.

The emulsions were subjected to oscillatory shear deformation using frequency sweep and strain amplitude sweep tests. The frequency sweep was carried out at a constant shear strain amplitude of 0.5%, by varying the angular frequency from 100 to 0.1 rad s^{-1}. The strain amplitude sweep test was carried out at a constant angular frequency of 10 rad s^{-1} and the amplitude was varied from 0.1 to 1000%. All measurements were carried out at 25 °C.

3D printing of emulgels. Direct ink writing (DIW)-based 3D printer (BIO X, CELLINK, Sweden) with a pneumatic printing head was used to fabricate a three-dimensional object using the printable emulgels. The device utilized 3 mL pneumatic syringe provided by CELLINK and sterile blunt needles (plastic, Drifton, Denmark). The nozzle size of the needle was 0.51 mm for all samples. Given designs were printed on a plastic Petri dish using rectilinear infill patterns and 10–25% infill density. Based on an initial optimization, the moving speed of the printhead was 8 mm s^{-1}, the extrusion speed was 0.012 mm s^{-1}, and the extrusion pressure was controlled in the range of 20–40 kPa.

Classical molecular dynamics simulation (CMDS). The α-chitin crystal and cellulose nanocrystals was constructed and the CMD simulations described in this study are shown in the ESI.†

Free fatty acid (FFA) release and hydrolysis kinetics analysis

Details of simulated gastrointestinal tract (GIT) model are provided in the ESI.† FFA released from the small intestinal stage was measured using an automatic titrator (902, Metrohm, USA). The pH of the mixture was maintained at 7.0 using 0.1 M NaOH, and the FFA release was determined according to the following equation:

$$\%\ \mathrm{FFA} = \frac{V_{\mathrm{NaOH}} \times m_{\mathrm{NaOH}} \times M_{\mathrm{Lipid}}}{W_{\mathrm{Lipid}} \times 2} \times 100$$

where V_{NaOH} was the consumed 0.1 M NaOH volume required to neutralize the FFAs (mL), m_{NaOH} is the NaOH solution molarity (0.1 M), M_{Lipid} and W_{Lipid} represent the molecular of sunflower oil (~250 g mol^{-1}) and total lipid weight (g).

In most emulsions, the released FFA tended to increase gradually over time during the intestinal digestion process,

potentially reaching the maximum FFA release (Φ_{max}). The kinetic parameters for the initial FFA release were calculated using equation[40]

$$\mathrm{In}[(\Phi_{max} - \Phi_t)/\Phi_{max}] = -kt + b$$

where k is the first-order rate constant for FFA release (s^{-1}) and t is the digestion time (s). The total FFA release level (Φ_{max}) was obtained from the FFA released curves.

Conclusions

Attractive Pickering emulgels (APEGs) were engineered by finely tuning interdroplet interactions at the colloidal scale through electrostatic attractions between CNC in the aqueous phase and interfacially adsorbed ChNF, using a sequential addition method. This approach led to the formation of flocculated and interconnected droplets that formed a three-dimensional network, imparting gel-like properties to the emulsion. Molecular dynamics simulations supported a bridging mechanism crucial for this system. The ChNF/CNC interparticle complexation was applicable across a broad range of APEGs, spanning from 40 to 70 wt% oil fractions, which led to different FFA digestibility. This study provides valuable insights into the interfacial dynamics between cellulose nanocrystals and chitin nanofibers, particularly their role in the micro-clustering of droplets, with implications for delaying lipid digestion. We anticipate that the strategy used in formulating APEGs could be extended to other sets of green nanoparticles exhibiting attractive interactions, opening opportunities relevant to the food and pharmaceutical fields.

Author contributions

Y.Lu and S.G. conceptualized the work. S.G. prepared ChNF and APEGs, performed TEM, fluorescence microscopy, rheology, and droplet size, interpreted the results, and wrote the manuscript. Y.Liu performed QCM-D tests. X.N. and J.X. analyzed the deacetylation degree of chitin. Z.W. performed the molecular dynamics simulations. W.J., J.Z., S.G., and L.H. performed GIT design and FFA release. L.B. and X.N. prepared ChNF and analyzed the morphology. J.L., J.X., B.L. and O.J.R. provided resources. L.B. and Y.Lu reviewed and revised the manuscript. O.J.R. supervised the work, reviewed and revised the manuscript. All authors have given approval to the final version of the manuscript.

Data availability

The data supporting this article have been included as part of the ESI.† The data that support the findings of this study are available from the corresponding author, Y.L. and O.J.R., upon reasonable request.

Conflicts of interest

The authors declare that they have no known competing financial interests or personal relationships that could have appeared to influence the work reported in this paper.

Acknowledgements

This work was supported by the Canada Excellence Research Chair initiative (CERC-2018-00006), and Canada Foundation for Innovation (Project Number 38623). S. G. acknowledges the foundation grant (No. GZKF202229) of State Key Laboratory of Biobased Material and Green Papermaking, Qilu University of Technology and Shandong Academy of Science. Y. Lu acknowledges the "Hundred Talents Program" of the Chinese Academy of Sciences. The UBC Bioimaging facility is also acknowledged for fluorescence microscopy imaging (RRID: SCR_021304).

References

1 X. Niu, Z. Wan, S. E. Mhatre, Y. Ye, Y. Lu, G. Gao, L. Bai and O. J. Rojas, *ACS Nano*, 2023, **17**, 25542–25551.
2 W. Liu, B. Pang, M. Zhang, J. Lv, T. Xu, L. Bai, X. M. Cai, S. Yao, S. Huan and C. Si, *Aggregate*, 2024, **5**, e486.
3 X. Yan, B. Wu, Q. Wu, L. Chen, F. Ye and D. Chen, *Energies*, 2021, **14**, 6077.
4 Y. Ming, Y. Xia and G. Ma, *Aggregate*, 2022, **3**, e162.
5 L. Bai, S. Huan, Y. Zhu, G. Chu, D. J. McClements and O. J. Rojas, *Annu. Rev. Food Sci. Technol.*, 2021, **12**, 383–406.
6 L. Huang, C. Xu, W. Gao, O. J. Rojas, W. Jiao, S. Guo and J. Li, *Carbohydr. Polym.*, 2024, **324**, 121541.
7 D. J. McClements, *Curr. Opin. Colloid Interface Sci.*, 2012, **17**, 235–245.
8 P. L. Fuhrmann, S. Breunig, G. Sala, L. Sagis, M. Stieger and E. Scholten, *J. Colloid Interface Sci.*, 2022, **607**, 389–400.
9 S. Cui, D. J. McClements, X. He, X. Xu, F. Tan, D. Yang, Q. Sun and L. Dai, *Food Hydrocolloids*, 2024, **146**, 109285.
10 B. Wu, C. Yang, Q. Xin, L. Kong, M. Eggersdorfer, J. Ruan, P. Zhao, J. Shan, K. Liu, D. Chen, D. A. Weitz and X. Gao, *Adv. Mater.*, 2021, **33**, e2102362.
11 X. Dai, J. Zhang, X. Bao, Y. Guo, Y. Jin, C. Yang, H. Zhang, L. Liu, Y. Gao, C. Ye, W. Wu, C. Liu, C. X. Zhao, J. Sheng, E. Ren, H. Li, W. Fang, B. Wu, J. Ruan, Z. Gu, D. Chen and P. Zhao, *Adv. Mater.*, 2023, **35**, e2303542.
12 M. Anvari and H. S. Joyner (Melito), *Food Res. Int.*, 2017, **102**, 1–7.
13 Y. Wang, C. Bai, D. J. McClements, X. Xu, Q. Sun, B. Jiao, Q. Wang and L. Dai, *Food Hydrocolloids*, 2023, **145**, 109097.
14 H. Katepalli, V. T. John, A. Tripathi and A. Bose, *J. Colloid Interface Sci.*, 2017, **485**, 11–17.
15 C. Qiu, C. Wang, X. Li, S. Sang, D. J. McClements, L. Chen, J. Long, A. Jiao, J. Wang and Z. Jin, *Food Hydrocolloids*, 2023, **135**, 108128.

16 S. Huan, M. Ago, M. Borghei and O. J. Rojas, *Cellul. Sci. Technol.*, 2018, 393–421.
17 Y. Lu, Y. Chun, X. Shi, D. Wang, F. Ahmadijokani and O. J. Rojas, *Adv. Mater.*, 2024, **36**, 2400311.
18 F. V. Ferreira, A. G. Souza, R. Ajdary, L. P. de Souza, J. H. Lopes, D. S. Correa, G. Siqueira, H. S. Barud, D. d. S. Rosa and L. H. Mattoso, *Bioact. Mater.*, 2023, **29**, 151–176.
19 Y. Lu, M. Mehling, S. Huan, L. Bai and O. J. Rojas, *Chem. Soc. Rev.*, 2024, **53**, 7363–7391.
20 X. Yu, X. Li, S. Ma, Y. Wang, W. Zhu and H. Wang, *Adv. Funct. Mater.*, 2023, **33**, 2214911.
21 B. Pang, H. Liu and K. Zhang, *Adv. Colloid Interface Sci.*, 2021, **296**, 102522.
22 C. Fu and M. Xu, *Green Carbon*, 2023, **1**, 43–46.
23 S. Guo, X. Li, Y. Kuang, J. Liao, K. Liu, J. Li, L. Mo, S. He, W. Zhu, J. Song, T. Song and O. J. Rojas, *Carbohydr. Polym.*, 2021, **253**, 117223.
24 L. Bai, L. Liu, M. Esquivel, B. L. Tardy, S. Huan, X. Niu, S. Liu, G. Yang, Y. Fan and O. J. Rojas, *Chem. Rev.*, 2022, **122**, 11604–11674.
25 M. Wu, P. Zhang, M. Li, R. Xu, X. Zheng, Q. Cui, R. Cha and B. Li, *ACS Appl. Mater. Interfaces*, 2023, **15**, 43468–43478.
26 W. Tian, X. Wang, Y. Ye, W. Wu, Y. Wang, S. Jiang, J. Wang and X. Han, *Green Chem.*, 2023, **25**, 10304–10337.
27 X. Li, Y. Kuang, Y. Jiang, H. Dong, W. Han, Q. Ding, J. Lou, Y. Wang, T. Cao, J. Li and W. Jiao, *Carbohydr. Polym.*, 2022, **277**, 118835.
28 S. Huan, Y. Zhu, W. Xu, D. J. McClements, L. Bai and O. J. Rojas, *ACS Appl. Mater. Interfaces*, 2021, **13**, 12581–12593.
29 S. Lv, H. Zhou, L. Bai, O. J. Rojas and D. J. McClements, *Food Hydrocolloids*, 2021, **113**, 106451.
30 S. Guo, Y. Zhu, W. Xu, S. Huan, J. Li, T. Song, L. Bai and O. J. Rojas, *Carbohydr. Polym.*, 2023, **299**, 120154.
31 S. Guo, L. Bai, J. Li, R. Bi, S. Huan and O. J. Rojas, *ACS Sustainable Chem. Eng.*, 2022, **10**, 9066–9076.
32 X. Su, Z. Wan, Y. Lu and O. Rojas, *Langmuir*, 2024, **40**, 4881–4892.
33 M. Massicotte and E. D. Cranston, *ACS Sustainable Chem. Eng.*, 2022, **10**, 14914–14925.
34 S. Yu, Y. Lu, S. Guo, T. Guo, A. Takagi, M. Kamkar and O. J. Rojas, *ACS Sustainable Chem. Eng.*, 2023, **11**, 12503–12513.
35 K. Hyun, S. H. Kim, K. H. Ahn and S. J. Lee, *J. Non-Newtonian Fluid Mech.*, 2002, **107**, 51–65.
36 Y. Lu, M. Kamkar, S. Guo, X. Niu, Z. Wan, J. Xu, X. Su, Y. Fan, L. Bai and O. J. Rojas, *Small*, 2023, **19**, e2300686.
37 D. Filip, V. I. Uricanu, M. H. G. Duits, D. van den Ende, J. Mellema, W. G. M. Agterof and F. Mugele, *Langmuir*, 2006, **22**, 560–574.
38 P. L. Fuhrmann, G. Sala, M. Stieger and E. Scholten, *Food Res. Int.*, 2019, **122**, 537–547.
39 W. Jiao, L. Li, A. Yu, D. Zhao, B. Sheng, M. Aikelamu, B. Li and X. Zhang, *J. Agric. Food Chem.*, 2019, **67**, 927–934.
40 Z. Ye, C. Cao, Y. Liu, P. Cao and Q. Li, *J. Agric. Food Chem.*, 2018, **66**, 6227–6238.